Available online at www.sciencedirect.com
SCIENCE DIRECT®
Thin Solid Films 500 (2006) 152 – 163
thin solid films
www.elsevier.com/locate/tsf

Correlation of atomic force–distance microscopy and spectrophotometric techniques in the analysis of optical multilayer spectral aging process

N.K. Sahoo *, S. Thakur, R.B. Tokas, M. Senthilkumar

Spectroscopy Division, Bhabha Atomic Research Centre, Trombay, Mumbai 400 085, India

Received 9 December 2004; received in revised form 12 July 2005; accepted 28 November 2005

Abstract

Aging-related multilayer spectral instabilities can pose severe performance limiting constraints to optical multilayer devices. In this study such instabilities of some periodic Gd_2O_3/SiO_2 optical multilayer systems have been explored using scanning probe force–distance microscopy and spectrophotometric techniques. In the present case, a strong correlation between the spectral instabilities *and* the viscoelastic properties of the associated thin film layers has been distinctly noticed. From the experimental analysis it was quite evident that the spectral instability, which starts during the nucleation and growth stage in thin films, continues to persist at a much longer time scale following aging processes. In this study it is shown that the elastic properties of the constituent thin films, the layer design and the bilayer thickness have established a strong interrelation which ultimately contributes to the multilayer instabilities. These spectral instabilities also have strong interconnections with the morphological and viscoelastic changes in such multilayers. Other multilayer parameters like the total number of layers, the layer structure, the microroughness evolutions, related stiffness factors and the adhesion properties of the periodic layer systems contribute substantially to this instability process.

PACS: 42.79.W; 78.66; 61.16.C
Keywords: Force–distance microscopy; Optical multilayer; Post-growth aging process; Optical coating; Multilayer morphology; Scanning probe microscopy

1. Introduction

Stabilities in thin film multilayer and superlattice systems have been very challenging and thought-provoking topics both from the application point of view as well as pedagogical interest [1–4]. A large number of interdependent parameters of the multilayer system always add to the complexity both in understanding and analyzing the instabilities. There are primarily two different kinds of instabilities in multilayer thin films one of which occurs during the growth stage and the other evolves under temporal aging conditions [5,6]. Although the instability characteristics of these two occurrences may be substantially different, a strong correlation between the initiation as well as evolution of these processes that occur at different time scale has been noticed. Since different multilayer developments adopt different material components, fabrication processes and layer geometries, an appropriate technique is required for probing particular and desired aspects of such instabilities. The present study is mainly dedicated to investigate and analyze spectral aging related instabilities of certain Gd_2O_3/SiO_2 periodic optical multilayer systems using force–distance curves obtained from atomic force microscopy and spectrophotometric techniques. Both these characterization techniques, especially scanning probe force–distance microscopy have become fundamental tools in several fields of research, such as surface science, material engineering, biochemistry and biology [7]. In the present work, we have extended their applications to the field of multilayer thin film optical coatings and observed a very useful feed back which helped us to understand the post-growth aging-related spectral, morphological and elastic instabilities of certain ultraviolet and deep ultraviolet multilayer systems. Although the data presented in this paper belong to a specific multilayer geometry, these can be conveniently extrapolated for several such periodic systems that use refractory thin film oxides in the optical multilayer structure. Besides, in periodic quarterwave multilayer systems the spectral parameters acquired through spectrophotometric technique can provide voluminous information on

* Corresponding author. Fax: +91 22 5505151.
E-mail address: nksahoo@apsara.barc.ernet.in (N.K. Sahoo).

0040-6090/$ - see front matter © 2005 Elsevier B.V. All rights reserved.
doi:10.1016/j.tsf.2005.11.109

the growth, as well as post-growth, especially aging-related instabilities. Such spectral parameters like bandwidth (FWHM) and reflectance amplitude (R_{MAX}) of quarter-wave-thick periodic multilayer system possess a well-defined functional relationship between themselves [8]. Post-growth compositional changes due to environmental effects show certain predictable functional trend in the reflectance bandwidth as well as spectral peak amplitudes of the multilayers [9]. Qualitative variation in spectral properties other than such compositional changes can be conveniently attributed to either morphological, viscoelastic changes or stress-driven instabilities [1]. For most of our Gd_2O_3/SiO_2 optical multilayers similar correlation between morphological instabilities and viscoelastic parameters have been noticed. In such situation scanning probe force–distance microscopy has a tremendous potential in probing various aspects of the elasticity related effects [10]. In this work several important parameters of this technique such as contact-lines, jump-to-contact, jump-off-contact and their slopes (stiffness factors) have been utilized to analyze the elastic and viscoelastic changes of the multilayers associated with the post-growth spectral instabilities. It is interesting to note from the experimental results that there exists a strong correlation between the scanning probe force microscopic results and the spectrophotometric values, although measurement variables, analysis techniques and operating principles are quite different. A brief overview of these techniques is presented in the subsequent sections. We have also shown in this work that elastic and microstructural properties are mathematically associated intimately with the spectral, physical and geometrical parameters of the multilayer structures.

2. Elastic properties and multilayer instabilities

The elastic properties of the constituent film materials have strong influences on various aspects of the stability of multilayer structures [7,11]. Such aspects include instabilities during growth and post-growth (aging) stages as well as stress-induced morphological instabilities [3–6,12–16]. There have been quite a few very interesting theoretical papers discussing various modeling aspects supporting some of the available experimental data [1,2,17,18]. Some research works on multilayer systems also suggested that elastic stresses could induce morphological instabilities leading to formation of islands, nonplanar surfaces, in some cases, the formation of deep, cusplike morphologies [10]. Such morphologies can provide *a* source for the nucleation of stress-relieving dislocations [19–21]. The wavelength of this type of instability is set by the competition between the stabilizing influences of the surface energy and the destabilizing influence of the misfit-induced elastic strain energy. The work of Sridhar and coworkers presents very detailed discussions on these aspects [2]. They have considered an infinite periodic and symmetric system with multilayer dynamics controlled by interfacial diffusion and focused only on specific interior layers that are far away from both the surface and the substrate.

There is also an extensive theoretical research paper by Huang and Desai on stress-driven instability in growing multilayer films [1]. Their work proposes a recursive procedure and a continuum, dynamic model to describe morphological evolution in coherent multilayer structures during the epitaxial growth. Some studies were also carried out by Shilkrot and coworkers on surface diffusion and morphological evolution with respect to the stability of multilayer systems [3,6,20]. In the course of our investigations on the instabilities, we have also noticed substantial changes in the evolution of morphology and grain structure in various Gd_2O_3/SiO_2 multilayer systems as well. For a system of stacked coherent strained islands (strained/spacer multilayers), in the work of Tersoff and coworkers [4], each buried island is approximately treated as a point defect, and its contribution to surface strain is determined by using continuum elasticity solutions of Maradudin and Wallis [22].

However, the theoretical analyses of Sridhar and coworker, have posed a more directional approach in predicting the multilayer stability based on material elastic and interfacial diffusion properties [2]. In the present experimental work we have adopted this elastic approach to explain the origin of instability in the Gd_2O_3/SiO_2 multilayer systems. Subsequently, we have noticed that elastic parameters only cannot explain the post growth instabilities unless one considers the complete multilayer geometry including the total number of layers. So more theoretical insight to this problem is essential to explain the experimental observations like ours, in which layer number dependent instabilities are specifically highlighted as well as dominated in the measurements. However, in this paper we have confined ourselves to the experimental observations and their analysis only, with the help of the available elastic effect related theoretical modeling proposed by Sridhar and coworkers [2]. As per this multilayer instability theory, when the thicknesses of the constituent layers are comparable, the elastic interactions between them cannot be ignored. The growth related elastic parameter α of such typical periodic bilayer system is given by [2]:

$$\alpha = \frac{E_A - E_B}{E_A + E_B} \tag{1}$$

where, E_A and E_B are the elastic moduli of the materials A and B respectively. In our present multilayer systems, gadolinium oxide (Gd_2O_3) with high refractive index is considered as a material A and silicon dioxide (SiO_2) with low refractive index value as material B. Both these films were deposited at a substrate temperature of 70 °C using reactive electron beam deposition process as described in the experimental section. The multilayer elastic growth function g that depends on the bilayer thickness and on the above elastic parameters can be given by [2,23]:

$$g(\alpha,f) = 12\alpha(1-\alpha) \times \frac{[3(1-3f+3f^2)\alpha^2 + 3(1-3f+3f^2)\alpha - 2(1-2f)]}{[1-\alpha(1-2f)]^2[1-\alpha^2(1-3f+3f^2)]} \tag{2}$$

where, the thickness fraction is $f = h/H$ and H is the total bilayer thickness or the overall wavelength of the multilayer, h is the thickness of the component layer A, and the thickness of the associated film material B is $(H-h)$. In this equation, both types

of layers are assumed to be isotropic and linear elastic media with different elastic constants. For a small wavelength limit, the total growth rate is negative provided the growth function $g(\alpha,f) \leq 0$ [2]. Consequently for specified relative thickness f, a flat interface in the multilayer system will be stable for a range of α values. It also can be seen that for a volume fraction less than ½, the flat interface is unstable for $0<\alpha<\alpha_c$ and stable for all other α, where α_c is its critical value. For a quarterwave optical multilayer stack, the physical thickness of the high index layers (A) are less than the low index (B) counterpart, hence the volume fraction for such materials is less than ½ as required by the above criterion. Also in our present Gd_2O_3/SiO_2 system the value of $g(\alpha,f)$ is computed to be -0.1840, which very well satisfies the requirements of the above equation. The critical elastic control parameter α_c of the bilayers related to $f(=h/H)$ of such a system is given by [2]:

$$\alpha_c = \frac{3(1-3f+3f^2) - [(1-3f+3f^2)(1+5f-5f^2)]^{1/2}}{2(1-2f)(1-3f+3f^2)} \tag{3}$$

As pointed out earlier, the origin of such a parametric function is based on the fact that when sub-layer thicknesses are comparable, elastic interactions between them have to be taken into the account. Such a relationship also focuses mostly on those layers which are not too close to either the free surface or the substrate. This equation also very interestingly depicted a strong functional behaviour of bilayer thickness or f-factor dependent instabilities.

The critical elasticity related parameter α_c has several significances in interpreting multilayer instabilities as it directly deals with interface elastic properties. Obviously, the only deficiency in the above theoretical modeling is the lack of functional dependence with respect to the total number of layers in a multilayer structure. In our present experimental studies it is quite apparent that a combination of elastic properties and total number of layers decide the stability criterion especially in the unstable regions of the multilayer geometry. For periodic quarter-wave optical multilayer, the optical thickness, which is a product of the refractive index, and the physical thickness is one-fourth (1/4) of the central wavelength (λ) of the devices [8,24], i.e.,

$$n_A(\lambda)h = \frac{\lambda}{4} = n_B(\lambda)(H-h) \tag{4}$$

From this expression, the physical thickness values of the associated layers can be easily derived. The dispersive refractive index profiles of Gd_2O_3 and SiO_2 correspond to $n_A(\lambda)$ and $n_B(\lambda)$ respectively. With these refractive index values and the corresponding physical thicknesses, the wavelength dependent elastic control parameters α_c can be easily expressed in terms of the refractive indices of the constituent materials as follows. Using the Eq. (4), the f-factor can be expressed as:

$$f = \frac{h}{H} = \frac{n_B(\lambda)}{\{n_A(\lambda)+n_B(\lambda)\}} \tag{5}$$

With a little mathematics to this relationship, the expression for α_c can be given by:

$$\alpha_c = (n_A+n_B) \times \left[\frac{3\left(n_A^2+n_B^2-n_An_B\right) - \left[\left(n_A^2+n_B^2-n_An_B\right)\left(n_A^2+n_B^2+7n_An_B\right)\right]^{1/2}}{2(n_A-n_B)\left(n_A^2+n_B^2-n_An_B\right)}\right] \tag{6}$$

This is very interesting equation, where the critical elastic parameter α_c is expressed in terms of the film microstructural parameters which are the refractive indices of the component films. Such an expression also clearly points out the interdependence between the microstructural properties and spectral parameters in a multilayer thin film system. In the above expression, the wavelength dependence of refractive indices is also got reflected in critical elastic coefficient values. The following section presents the experimental details of the sample preparation as well as characterizations through multimode scanning probe microscopy and spectrophotometry.

3. Experimental details

Several multilayer filters have been designed and developed for various excimer laser wavelengths using Gd_2O_3 as high index and SiO_2 as low index layers. Such reflecting filters include (i) a 41-layer reflector for 193 nm ArF Laser, (ii) 31 and 14-layer reflection filters for 222 nm KrCl laser, (iii) a 25-layer reflector for 248 nm KrF laser and (iv) a 21-layer multilayer for 355 nm XeF laser. Such wide varieties of designs were tried out in order to study the systematic changes in the spectral and viscoelastic instabilities of these dielectric ultraviolet and deep ultraviolet multilayer reflectors over a period of time.

Under the present investigation, we have carried out some systematic experiments and analysis on post-growth aging related instabilities of these multilayers using a multimode scanning probe and spectrophotometric techniques. The samples were deposited in a fully automatic thin film vacuum system "VERA-902" by adopting the reactive electron beam deposition technique. The depositions of the films were carried out using an 8 kW electron beam gun with sweep and automatic emission controls. The film materials for SiO_2 and Gd_2O_3 were chosen from Cerac's batch number "S-1060" (purity 99.99%) and "G-1076" (purity 99.9%) respectively. The substrate temperature was maintained at 70 °C for all the deposited films. The total pressure inside the chamber during the deposition process was maintained at $\sim 1\times10^{-4}$ Torr through appropriate mass flow controllers. The constituents of the gases present during the deposition were analyzed by a residual gas analyzer model; Pffeier's Prisma-200. The film thicknesses were monitored using both the Leybold's OMS-2000 optical thickness monitor as well as Inficon's XTC/2 quartz crystal monitors. The typical rate of depositions was maintained at 1 nm/s for most of the films. The entire deposition process parameters such as substrate temperature, rate of deposition, total reacting gas pressure were monitored and controlled by a Siemen's industrial programmable logic

controller with appropriate front-end software. The film thicknesses were kept constant at quarter wave thickness at the respective laser wavelength. For 248 nm (KrF laser) wavelength this amounts to be approximately 31 nm for Gd_2O_3 and 42 nm for SiO_2 layers in terms of their physical thicknesses.

For AFM characterization, NT-MDT's solver P-47H multi-mode ambient-based scanning probe system has been utilized. The cantilever used was a Si_3N_4 with typical spring constant of 0.6 N/m and resonant frequency of 75 kHz. We have adopted the contact mode operation without any image filtering technique for the topographic measurements. For Fourier analysis, the built-in fast Fourier transform module of the control software "NOVA-SPM" was employed to generate the mappings. In order to have the consistency in the experimental results, the same cantilever was used for all the force–distance microscopy measurements. All the multilayers were spectrally measured for their reflectance as well as transmittance characteristics using Shimadzu UV3101PC uv–vis–nir spectrophotometer system. Spectral characteristics were recorded initially just after the development and subsequently after 6 months, in order to observe the spectral changes/instabilities with respect to aging under normal ambient conditions. It was noticed that the multilayers terminated with low index SiO_2 layer have shown relatively more aging related degradation in spectral characteristics than the structure ended with Gd_2O_3 layers.

4. Multilayer instabilities and force–distance microscopy

Atomic force microscopy concerns with the fundamental interactions between surfaces extends across physics, chemistry, materials science and a variety of other disciplines [7,25]. Since 1989, this technique has emerged as an essential tool for studying surface interactions by means of force–distance curves which is otherwise known as scanning probe force microscopy [25,26]. With force sensitivity of the order of a few piconewtons, AFMs are excellent tools for probing these fundamental force interactions, especially, when adhesion are gaining more and more attention with the development of micro- and nanotechnologies [27,28].

In a typical force-microscopy, during the approach of the AFM-tip to a solid sample surface, a "jump-to-contact" instability occurs before zero distance with an undeflected

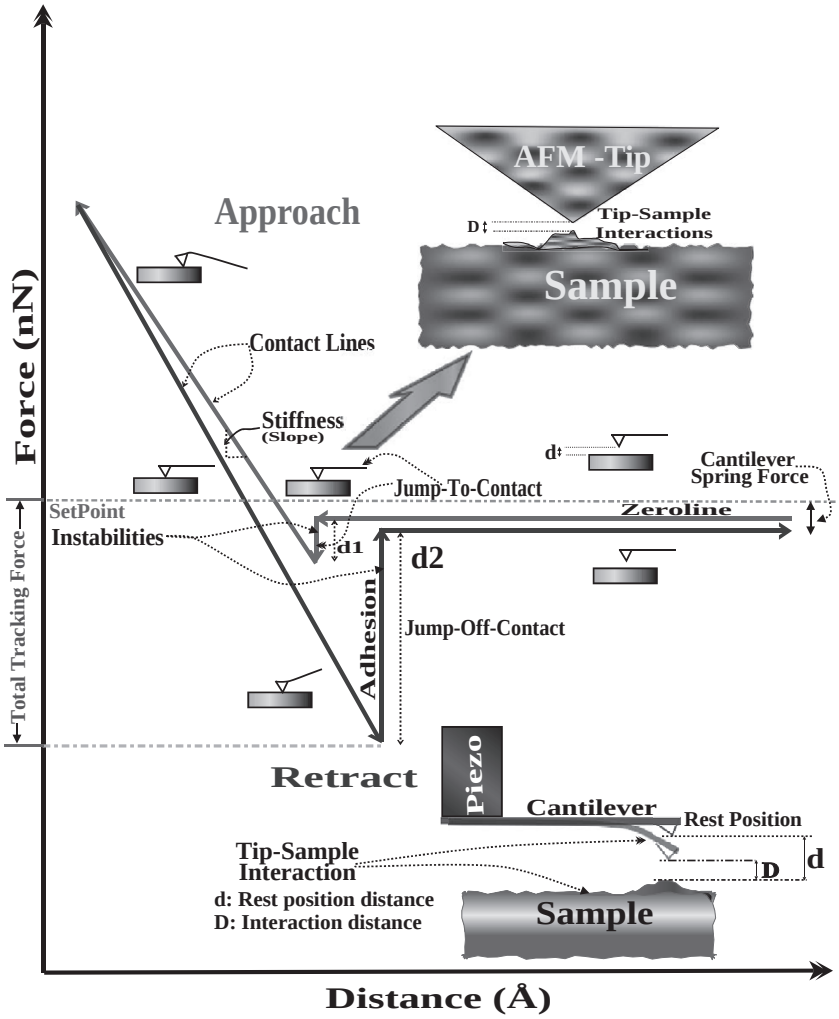

Fig. 1. Schematic of force–distance microscopic measurements depicting various important characteristics in the loading and unloading processes in force–distance curve.

cantilever is reached. During retraction of an AFM-tip pressed against the sample surface, it adheres to the surface until the spring force of the cantilever is higher than the attractive interaction force and undergoes a second instability in terms of "jump-off-contact". These two instabilities, which represent the interaction forces between the sample and the probe, strongly depend on the mechanical, elastic and viscoelastic properties of the interacting materials [7,29–32]. Hence, the dynamical changes in the numerical values of these two instabilities provide voluminous information on the post-growth aging related instabilities of a multilayer system. A typical simulated force–distance curve usually obtained by AFM is depicted in Fig. 1. The force between the AFM tip and the surface is quantified along the vertical axis, while the horizontal axis shows the tip–surface displacement coordinate. There are several interesting as well very important regions of this force–distance or force–displacement characteristic [7] that has been utilized in this experimental work.

5. The three prime regions of the force–distance (F–D) curve

Both approach and withdrawal force–distance curves can be roughly divided into three prime regions: the contact line, the non-contact region and the zero line [7]. When the sample is pressed against the cantilever, the tip is in contact with the sample and $D=0$. The corresponding lines obtained in the force–displacement curve are called "contact lines" as depicted in Fig. 1. Usually, the contact lines provide information on sample stiffness. It is also possible to draw information about the electro-plastic behaviour of the materials from the contact lines of force. The origin (start point) of force–displacement curves is usually put at the intersection between the prolongation of the zero line and the contact line of the approach curve. When the sample is elastic in nature, the approach and retraction contact lines usually overlap. Since the most practical samples have mixed or intermediate elastic behaviour, the loading and the unloading curves seldom overlap as shown in Fig. 1. The difference between the approach and the withdrawal lines is called "loading–unloading-hysteresis". Referring to Fig. 1, the distances $d1$ and $d2$ are called "jump-to-contact distance" and "jump-off-contact distance". The adhesion work equals the area between the negative part of the withdrawal curve and the Z-axis. The hysteresis of the curve is the difference between the adhesion work and the area between the negative part of the approach curve and the Z-axis. The most interesting regions of force displacement curves are the two non-contact regions, containing the jump-to-contact and the jump-off-contact events. The non-contact region in the approach curves gives information about attractive or repulsive forces before contact. In particular, the maximum value of the attractive force sampled prior to contact equals the pull-on-force, i.e., the product of jump-to-contact and cantilever deflection. On the contrary, the pull-off force, i.e., the product of jump-off-contact deflection and cantilever force constant equals the adhesion force. In order to relate the tip sample surface energies and the adhesion force it is necessary to evaluate the deformations and the contact area of the samples. This can be done by means of different theoretical modeling [7].

5.1. Non-contact region in F–D microscopy

The non-contact region of the force–distance measurements contains very useful viscoelastic information on the tip–sample interaction forces. The experimentally observed dynamic changes to these forces can help in understanding the microstructural evolutions in thin films and multilayers. The outcome of such microstructural changes most often gets reflected in several instabilities, for example, spectral and morphological properties in this case. Following sections put some light to these aspects.

5.1.1. Approach curve: attractive forces and jump-to-contact

As mentioned earlier, the "jump-into-contact" is one of the important quantities that can be measured in a force–distance microscopy and it contains very important information on the viscoelastic properties of the interacting force field. It appears as a discontinuity when the gradient of the tip–sample force is larger than the elastic constant of the cantilever. The onset of a jump-to-contact is predicted by any theory that takes attractive forces in to account (JKR or Maugis) and is also predicted by several numerical calculation [7,33,34]. In AFM measurement the jump-to-contact instability is governed by the stiffness of the cantilever relative to the long-range tip–sample forces. If cantilever elastic constant is bigger than the maximum value of the tip–sample force gradient, then the discontinuity virtually disappear. However, jump-to-contact is always present at an atomic scale, even if the cantilever can be modeled as an infinitely rigid body [7]. In this case, jump-to-contact instability is governed by the stiffness of the tip and the sample materials and related to their cohesive strengths. This phenomenon has been demonstrated by Pethica and Sutton [35] with the help of calculations employing Lennard-Jones potentials and by Landman et.al [36] by use of molecular dynamics (MD) simulations.

In a simplified approach, when the tip is moved towards the surface, the total energy is initially entirely dominated by the elastic energy of the cantilever. Eventually, the attractive force becomes strong enough to impose the global energy minimum. A commonly used form of intermolecular potential V is the Lennard-Jones 6–12 potential given by [37–39],

$$V_{\mathrm{LJ}} = V_0\left[\left(\frac{x_0}{x}\right)^{12} - 2\left(\frac{x_0}{x}\right)^{6}\right] \tag{7}$$

A total potential function, consisting of the sum of the intermolecular and probe elastic function can be given as [39],

$$U_{\mathrm{LJ}}(x) = V(x) + \frac{1}{2}k(x-d)^2 \tag{8}$$

Where k is the spring constant of the cantilever and d is the position of the cantilever. The most eminent feature of the total potential function is the presence of two energy wells with a

barrier in between, for a wide range of k and d. Also these two energy function wells (minima) dynamically change during approach and retraction process. During probe approach, the probe well shrinks while the intermolecular well grows, the opposite occurs during the retraction process. When one well dominates the other the cantilever either jump-into or jump-off the equilibrium point, depending upon the potential function's shape and the dynamics. A typical effective interactive potential is depicted in Fig. 2. In this representative calculation the value of the spring constant k is taken as $0.3V_0/x_0^2$. It is important to note that two instabilities, jump-to-contact and jump-off-contact, depend strongly on the interacting potentials, which in turn depend on the elastic and viscoelastic properties of the sample and the cantilever.

Pethica and Sutton [35] have shown that in general there exists a minimum separation (~1–2 Å) below which the surfaces jump into contact irrespective of the rigidity of the holder. This instability is due to the fact that, at some small enough separation, the gradient of the surface forces exceeds the gradient of the elastic restoring bodies. The instability is irreversible because surface forces have stronger separation dependence than does the elastic restoring force. Lennard-Jones pair potential used by Pethica and Sutton [35] is inapplicable to free surface structures. N-Body potentials of the embedded atom variety are rather much more reliable in such cases. They do not, however, account for long-range attractive forces because they do not incorporate Van-der-Waals term. Landman et al. [36] verified the onset of jump-to-contact instability by means of molecular dynamics (MD) simulations. The inter-atomic interactions governing the energetic and dynamics of the system are modeled by means of embedded-atom method (EAM). In the EAM [40], the dominant contribution to the cohesive energy of the material is viewed as the energy to embed an atom in to local electron density provided by other atoms of the system. The presence of the energy barrier prevents the tip–cantilever system to interact. At the distance where the interactive force becomes equal to the cantilever constant, the local minimum due to cantilever elasticity disappears, and the probe abruptly moves to a new position, corresponding to the global minimum, which is the "jump-to-contact".

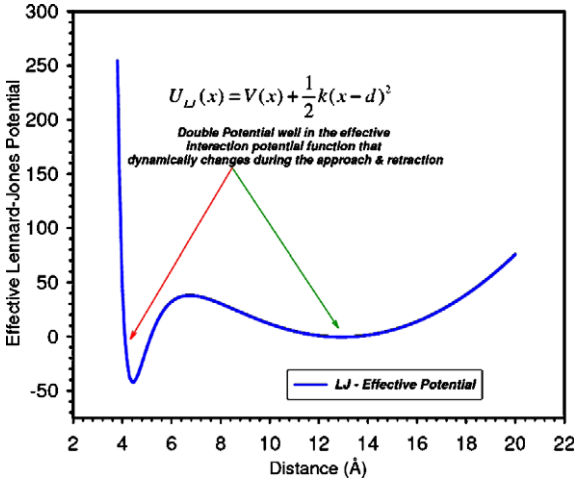

Fig. 2. Lennard-Jones potential computations depicting double potential well that contribute to the jump-in and jump-off contacts.

5.1.2. Withdrawal curve: jump-off-contact and adhesive forces

The second discontinuity or instability of force–displacement curves, the jump-off contact occurs when, during the withdrawal of sample, the cantilever elastic constant is larger than the gradient of tip–sample adhesive forces [7]. Unlike jump-in, the jump-off contact is related to tip and sample surface energies via equations that depend on materials dimensions, elasticity, stiffness and adhesion. The jump-off-contact deflection and its distance are usually greater than jump-to-contact deflection and the corresponding distance, respectively. This occurs for several reasons. When the tip is moved toward the surface, the total energy is initially entirely dominated by the elastic energy of the cantilever. Eventually, the attractive force becomes strong enough to impose the global energy minimum. The presence of the energy barrier prevents the tip–cantilever system from interacting. At the distance where the net force gradient, $F_T'(D)=k$, the local minimum due to cantilever elasticity disappears, and the probe abruptly moves to a new stable position (jump-off), corresponding to the global minimum. Hence the nature of these two discontinuities or instabilities if analyzed appropriately can reveal several information on the sample mechanical, compositional and viscoelastic properties [41]. The experimental force distance curves for an unstable 14-layer KrCl ($\lambda=222$ nm) laser reflecting multilayer system is presented in Fig. 3(a) and (b) depicting changes (instabilities) during the growth and post growth stages of a time interval of 6 months. It can be seen from these figures that not only the instabilities amplitudes but also their shapes are drastically different at the two different instances.

6. Analysis of instabilities through multilayer spectrophotometry

The spectrophotometry has been a very well known and established technique in probing the spectral response of an optical multilayer device. For a periodic quarterwave-thick multilayer system consisting of an alternative high (n_H) and low (n_L) refractive index, the width of the reflection band (FWHM) in terms of $w=\lambda_0/\lambda$ can be given by the expression [24],

$$\mathrm{FWHM} = 2\Delta w = \frac{4}{\Pi}\sin^{-1}\left(\frac{n_H - n_L}{n_H - n_L}\right) \tag{9}$$

where n_H, n_L are the refractive indices of the high and low index layers respectively. Also λ_0 and λ are the central and the scanning wavelengths respectively. Similarly, the maximum reflectance amplitude R_{MAX} of such a multilayer system is given by [24]:

$$R_{MAX} = \left(\frac{1-(n_H/n_L)^{2p}(n_H^2/n_S)}{1+(n_H/n_L)^{2p}(n_H^2/n_S)}\right)^2 \tag{10}$$

where $(2p+1)$ is the number of layers in the multilayer and n_S is refractive index of the substrate. Similar expressions also can be derived for even number of layers. It can be seen from both

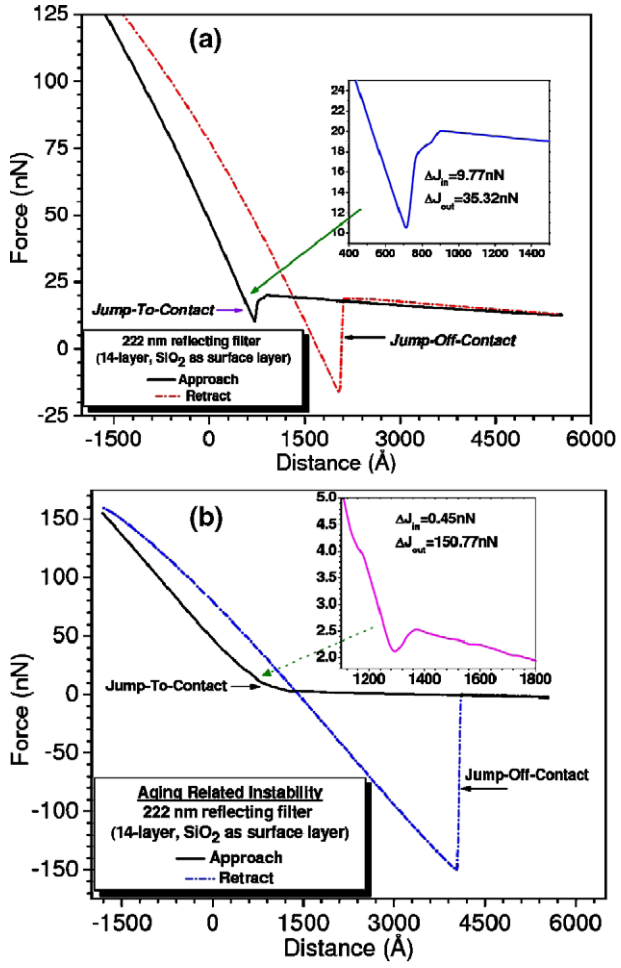

Fig. 3. Force–distance curve of a 14-layer unstable KrCl (222 nm) laser reflecting multilayer measured (a) immediately after the growth and (b) after a period of 6 months.

these equations that values for FWHM and R_{MAX} will have similar functional trend when the refractive index values for the two materials are either increased or decreased. That means, due to the environmental effect when the refractive indices of both the material increases, the two spectral parameters R_{MAX} and FWHM should increase and the vice versa. Besides, the overall spectral peak position should shift towards the higher wavelengths [42]. A typical simulation to the environmental related refractive index changes on the spectral properties of a 13-layer multilayer system is presented in Fig. 4. Effects other than the compositional changes due to the environmental effect may demonstrate different kinds of functional trend in the R_{MAX} and FWHM values like in our present multilayers. A few of such instabilities are stress driven, morphological, interfacial–inter diffusion related instabilities [2].

Mostly compositional (environmental) instability in oxide multilayers is associated with penetration of ambient moisture into the structure and alters the dielectric constant or refractive index (usually increase) of the individual layer system [43]. Such a change that affects the ratios of refractive indices has a very well defined impact on the multilayer spectral properties. These include the changes in bandwidth and the amplitude of the reflectance spectra of the quarterwave structures. It can be

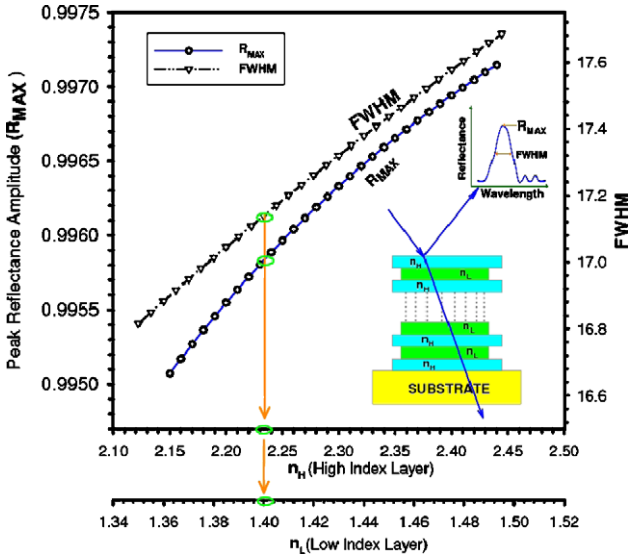

Fig. 4. Computed peak reflectance maximum (R_{MAX}) and the spectral band width (FWHM) of a 13-layer compositionally unstable multilayer varying both high (n_H) and low (n_L) refractive indices of the component layers. Each point of the R_{MAX} and FWHM curves corresponds to a definite pair of n_H and n_L values presented in the respective axes and it is demonstrated by the arrows as an example.

noticed from the above equations that amplitude and bandwidths are intimately interdependent and strongly associated with the refractive index ratios. Broadly speaking, under humidity induced compositional changes, values for both the bandwidth and the amplitude along with the spectral peak position should simultaneously increase [44] and it is primarily due to the increase in the dielectric constants of the associated thin film layers [45].

It is worth mentioning here that under our present investigations, an altogether different type of spectral variation has been noticed in most of the multilayer systems. This includes the increase in the reflectance amplitude with the decrease of FWHM, etc. Such anomalous changes in spectral

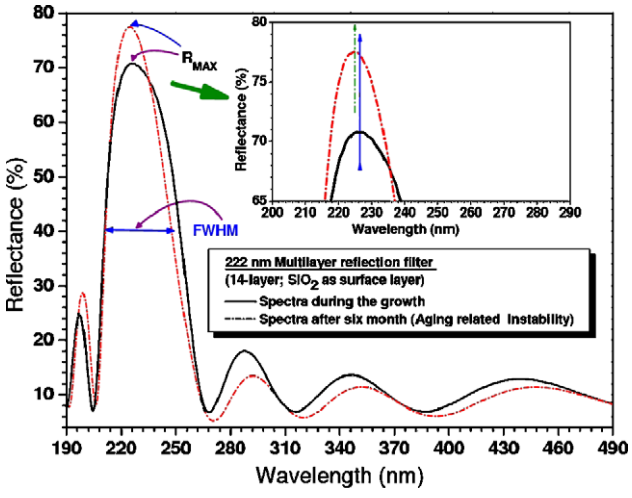

Fig. 5. Spectral R_{MAX} and FWHM measurements of the unstable 14-layer multilayer through spectrophotometry. The aging related measurements were carried out after an interval of 6 months. Inset figure depicts a slight shift in spectral peak position towards the shorter wavelength implying strain field related instability.

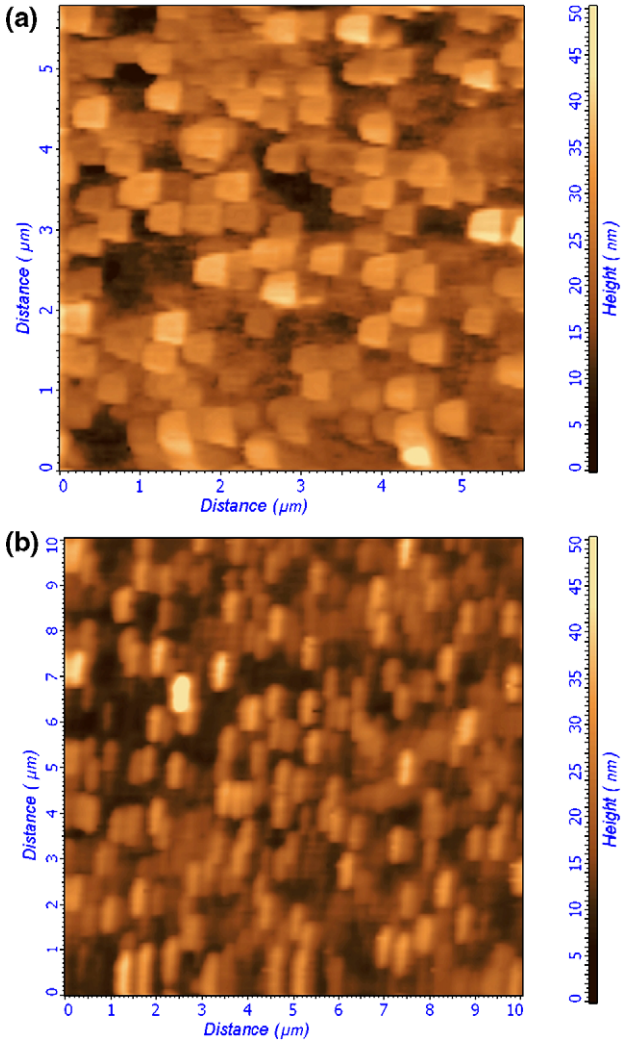

Fig. 6. AFM morphology of (a) as-deposited and (b) 6-month aged 14-layer unstable reflecting multilayer depicting notable changes in the grain structures.

properties may be attributed to the predominantly morphological, elastic or stress-driven instabilities. The experimental spectral measurements of an unstable 14-layer multilayer are depicted in Fig. 5. This figure shows both the growth and post growth (6 months later) aging-related spectral reflectance measurements results. As can be seen, the post growth instabilities have shown an increase in the reflectance amplitude of the stop band and a decrease in the value of its spectral width (FWHM). Besides, there is a small shift in the peak position towards shorter wavelength. Such changes cannot be explained through compositional instabilities as described earlier [44]. The topographic changes of this unstable multilayer system are depicted in Figs. 6(a) and (b). It can be observed in this figure that the morphology has been substantially altered with respect to the grain sizes as well as root mean square (RMS) roughness values. Such changes have distinctly pointed out the strong correlation between the spectral and morphological instabilities as discussed by several other experimental papers. It can be distinctly noticed from Fig. 6(b) that for the unstable multilayer there is substantial change in the grain structure size as well ordering. The grains which were cubic and more randomly distributed have subsequently demonstrated rectangular size and better ordering. Such ordering is very much similar to the self organization process induced by an effective strain field [46]. Spectral reflectance also depicted such strain field induced effect both in the amplitude as well as FWHM values.

These aspects also were reflected in the topographic and viscoelastic properties as measured through the force distance microscopy. The values of jump-to-contact and jump-off-contacts very interestingly follow a systematic as well as symmetric functional trend with respect to the spectral parameter changes. In the present paper, we have noticed a strong correlation between the scanning force spectroscopic results and the spectrophotometric values, although measurement, operating principles, analyses and mechanisms are quite different. The following sections discuss some of our experimental results and their analyses.

7. Results and discussions

Fig. 7(a) depicts the instabilities in spectral parameter with respect to changes in jump-to-contact forces in case of several periodic multilayers. The two curves represent the instabilities

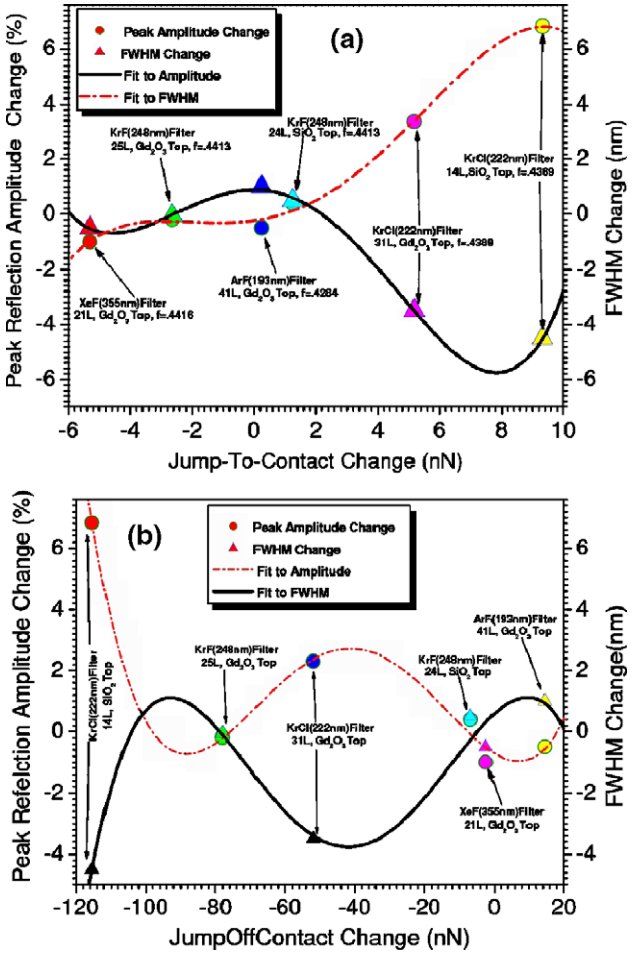

Fig. 7. Plots of changes in peak reflection amplitude and FWHM of Gd_2O_3/SiO_2 multilayers as a function of changes in (a) jump-to-contact and (b) jump-off-contact distances.

in the reflectance bandwidth (FWHM) and peak amplitudes respectively. It is interesting to note that for most of our multilayers these two spectral parameters have depicted opposite types of instabilities with varying magnitudes. Such changes, as discussed earlier, point out to the morphological or viscoelastic instability which is different from the compositional type. The data values in it are fitted with the appropriate polynomials in order to present smooth functional trend. The highest instability values were observed for a 14-layer KrCl (222 nm) reflecting multilayer, which has bilayer thickness of 64.77 nm (f=0.439). The 41-layer ArF (193 nm) reflecting filter with a bilayer thickness of 54.26 nm (f=0.428) also demonstrated a small amount of instability. Lower instabilities were recorded for 24-layer as well as 25-layer reflecting multilayers designed for KrF (248 nm) laser wavelength with a bilayer thickness of 73.48 nm (f=0.441). The quarter wave devices developed for this wavelength have depicted maximum stability [47]. Similarly, the 21-layer multilayer for XeF (355 nm) laser with bilayer thickness of 108.64 nm (f=0.447) has shown reasonably good stability.

Over all, the multilayers with smaller positive or negative changes in the jump-to-contact forces have depicted better stabilities. Fig. 7(b) depicted the spectral parameter instabilities with respect to the changes in the jump-off-contact forces. In this case also the same 14-layer (KrCl laser reflector) multilayer with the bilayer thickness of 64.6 nm depicted both the highest spectral instability as well as larger viscoelastic changes. The better spectrally stable KrF (248 nm) multilayers (bilayer thickness of 73.48 nm) showed discrete negative values in the change of jump-off-contact force variations depending on the multilayer geometry and the surface layer. The spectral data versus jump-off-contact values were fitted with a polynomial function to represent a smooth functional dependence. Both the curves showed systematic periodic variations where the stable multilayers are found to be positioned at or close to the node-like points. It is interesting to note from both these experimental results that the multilayer reflectors carrying bilayer thickness below a certain optimum value have shown maximum instability. That is, multilayers meant for 193 nm-ArF laser (bilayer thickness 54.26 nm, f=0.428) and 222 nm-KrCl laser (bilayer thickness 64.77 nm, f=0.439) have shown higher degrees of instabilities. Such observations depicted close relationships with the elastic properties and f-factors of the component film material as discussed by Sridhar and coworker.

We have computed the elastic coefficient α for the Gd_2O_3/SiO_2 bilayer system by considering some published elastic coefficients for these materials for our present substrate temperature values [48]. By taking elastic moduli of Gd_2O_3 and SiO_2 as 140.6 and 73.61 GPa respectively for the substrate temperature conditions of 70 °C, the α value can be computed as 0.312 using the Eq. (1). The critical value α_c of different multilayer system have been evaluated by using appropriate bilayer thicknesses (f-factors) from the refractive index values of the film material involved in the structure. The dispersive refractive index values for Gd_2O_3 and SiO_2 are depicted in Fig. 8. We have plotted the critical α_c versus wavelength of Gd_2O_3/SiO_2 system and noticed a dispersive behaviour as it can be seen from Fig. 9. The computed α value (=0.312) has been plotted as a straight line in this graph. It is interesting to see that the multilayers meant for ArF laser (193 nm) and KrCl laser (222 nm) wavelength have critical α_c values greater than the α value (=0.312) for the periodic quarterwave Gd_2O_3/SiO_2 multilayer systems. In spectral measurements also multilayers belong to these wavelengths have demonstrated strong instabilities. However, one of the contrasts that is observed in this analysis that the multilayers belonging to ArF laser (193 nm) should have had instability factors higher than the KrF laser (222 nm) mirrors, because of relatively more deviations in the elastic coeffi-

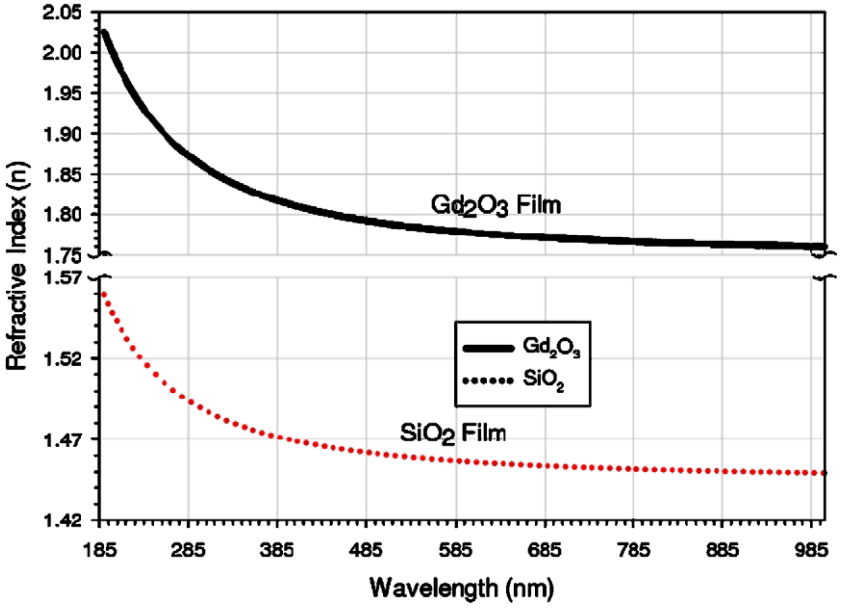

Fig. 8. Experimental spectral refractive index profiles of Gd_2O_3 (n_H) and SiO_2 (n_L) optical films deposited using reactive electron beam deposition technique.

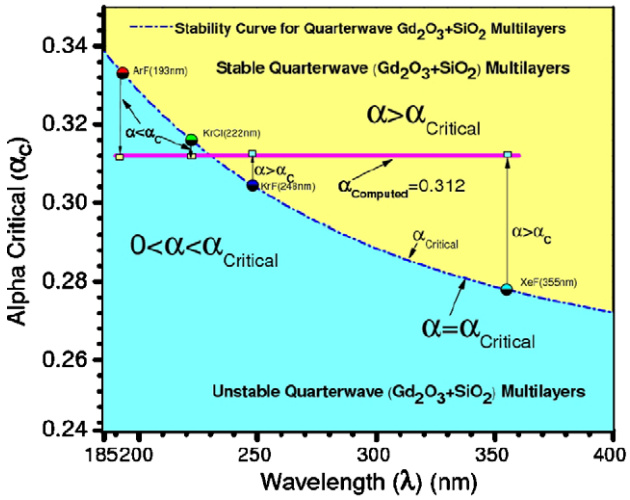

Fig. 9. Plot of computed values of α and experimental values of α_c for various Gd_2O_3/SiO_2 multilayers.

cients. Whereas the experimental spectral measurements have shown less instability in ArF laser reflectors than the KrCl laser multilayers. This may now be accountable to the total number of layers, which are different in these multilayer structures.

In order to investigate this instability aspect further, we have presented the jump-to-contact and jump-off-contact values for the unstable multilayers in Fig. 10. It can be noticed from this plot that both the viscoelasticity related jump-to-contact and jump-off-contact values have approached a minimum absolute value for the multilayers with *only* certain layer numbers in the geometry. The similar information can also be *obtained* from the graphs in Fig. 11 where spectral data are presented with respect to the layer numbers. It is noticed from this presentation that for elastically unstable multilayer system, the spectral instability can be reduced appreciably by choosing appropriate number of layers in the system. Some more interesting information on the adhesion and stiffness measurement results on various multilayer systems is presented in Figs. 12(a) and (b). In Fig. 12(a) it is interesting to note that the initial values (i.e., growth stage values) in adhesion and stiffness have depicted opposite

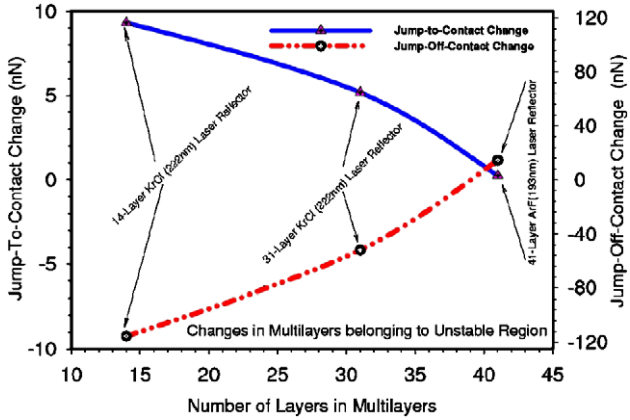

Fig. 10. Layer number dependent changes in jump-to-contact and jump-off-contact values for the unstable multilayers.

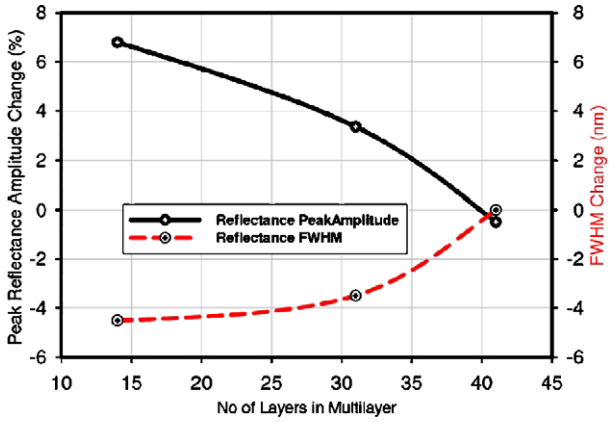

Fig. 11. Layer number dependent spectral parameter changes for unstable multilayers.

trends for various multilayers. Which means that the multilayers with better adhesions tend to have lower stiffness values and the vice versa. But for unstable multilayers, the jump-to-contact is found to be a very sensitive parameter to explain the present instability. In our case both 14-layer as well as 31-layer 222 nm (KrCl laser) reflecting multilayers depicted higher jump-to-contact values. The relationship between instabilities in stiffness and adhesion force for all

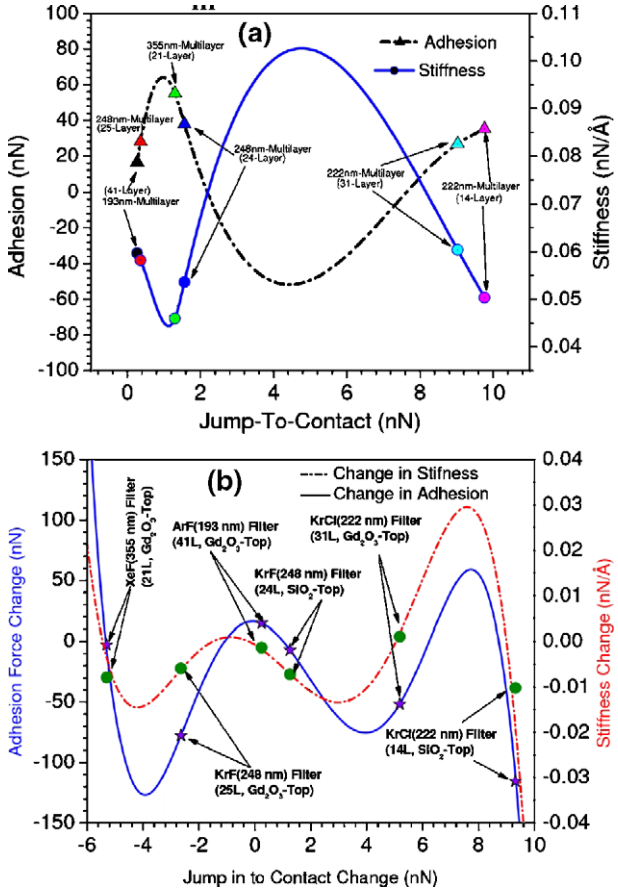

Fig. 12. (a) Changes in the stiffness and adhesion values with respect to jump-to-contact values for various stable and unstable multilayers and (b) during the evolution of the instabilities.

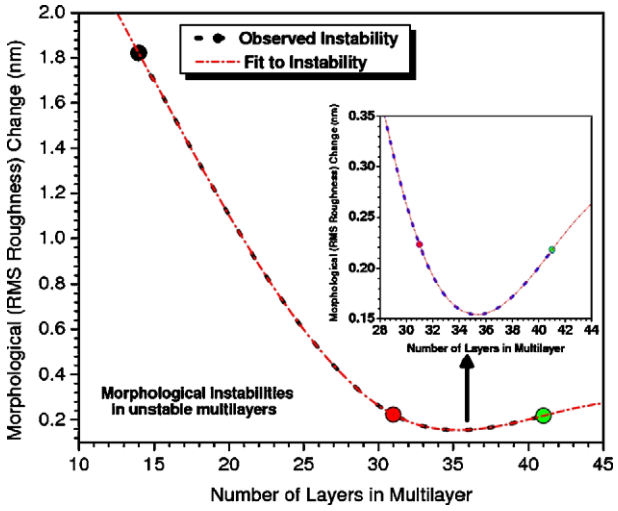

Fig. 13. Depiction of morphological instability in unstable multilayers. It can be seen that the changes in RMS roughness values for the unstable multilayers substantially decrease as the number of layers in a multilayer increased ultimately approaching an optimum value. The inset plot highlighted this aspect more distinctly.

of our multilayers with respect to jump-to-contact instabilities are depicted in Fig. 12(b). It is noticed here that change in adhesion and the stiffness factors (instabilities) both follow a very similar characteristic (trend) for various multilayer layer-structures and geometry. This indicates that stiffness and adhesion evolutions at a longer time scale (post growth stages) can follow each other.

The results on the morphological changes with respect to number of layers in the unstable multilayers are depicted in Fig. 13. It can be seen from this plot that the morphological changes are minimum for the unstable multilayer geometry with optimum number of layers. The inset picture highlights more this observation. These results also hinted towards the close association of morphological instability with the elastic and spectral instabilities in the multilayer systems. So for elastically unstable periodic bilayer systems it is always possible to achieve a better stability factors by appropriately choosing an optimum number of layers in the multilayer geometry. The stability factors in such multilayers improve most likely due to appropriate values in the stiffness and adhesion properties of the component layer systems.

8. Conclusions

The present work deals with the experimental investigations and analysis of the post growth aging-related instabilities aspects of Gd_2O_3/SiO_2 multilayer system based on scanning probe force microscopy and optical spectrophotometric results. During analysis a very good close correlation was noticed between the results of these techniques. It was interesting to note that the most important interaction phenomena, jump-to-contact and jump-off-contact, of the force–distance microscopy, which deals with elastic properties of materials, have agreed very well with the spectral properties acquired through the spectrophotometric techniques. It is a very good example of coexistence of diversified characterization and analysis approaches in probing and explaining instabilities in precision multilayer systems. The most elastic based theories that are applicable for the growth stage of the thin films can be conveniently applied to a much longer time scale of post growth aging-related instabilities. Besides the elastic properties of the component materials, the layer geometry, structures and the total number of layers have strong impacts on the multilayer instabilities. Most importantly, the layer number dependency has depicted a very strong influence to interpret the instability results. However such an important parameter has been completely neglected in the existing theoretical modeling and analyses. In the present experimental study it has been distinctly demonstrated that with the given material elasticity parameters, instability process can be minimized by choosing an optimum layer numbers in a specific periodic multilayer system. Hence the existing theoretical approaches have to be appropriately extended to accommodate more number of multilayer geometric information, especially layer number parameter, to explain various instability related experimental results.

References

[1] Z.F. Huang, R.C. Desai, Phys. Rev., B 67 (2003) 075416.
[2] N. Sridhar, J.M. Rickman, D.J. Srolovitz, J. Appl. Phys. 82 (1997) 4852.
[3] L.E. Shilkrot, D.J. Srolovitz, J. Tersoff, Appl. Phys. Lett. 77 (2000) 304.
[4] J. Tersoff, C. Teichert, M.G. Lagally, Phys. Rev. Lett. 76 (1996) 1675.
[5] S.F. Pellicori, E. Colton, Thin Solid Films 209 (1992) 109.
[6] L.E. Shilkrot, D.J. Srolovitz, J. Tersoff, Phys. Rev., B 62 (2000) 8397.
[7] B. Cappella, G. Dietler, Surf. Sci. Rep. 34 (1999) 1.
[8] S. Furman, A.V. Tikhonravov, Basics of Optics of Multilayer Systems, Frontier Editions, Gif-sur Yvette, 1992.
[9] S.F. Pellicori, H.L. Hettich, Appl. Opt. 27 (1988) 3061.
[10] W.H. Yang, D.J. Srolovitz, J. Mech. Phys. Solids 42 (1994) 1551.
[11] J. Mirecki-Millunchick, R.D. Twesten, D.M. Follstaedt, S.R. Lee, E.D. Jones, Y. Zhang, S.P. Ahrenkiel, A. Mascarenhas, Appl. Phys. Lett. 70 (1997) 1402.
[12] K.C. Hsieh, J.N. Baillargeon, K.Y. Chang, Appl. Phys. Lett. 57 (1992) 2244.
[13] K.Y. Cheng, K.C. Hsieh, J.N. Baillargeon, Appl. Phys. Lett. 60 (1992) 2892.
[14] S.T. Chou, K.Y. Cheng, L.J. Chou, K.C. Hsieh, J. Appl. Phys. 78 (1995) 6270.
[15] N.Y. Jin-Phillipp, F. Phillipp, T. Marschner, W. Stolz, J. Mater. Sci., Mater. Electron. 8 (1997) 289.
[16] D. Josell, W.C. Carter, J.E. Bonevich, Nanostruct. Mater. 12 (1999) 387.
[17] A. Ponchet, A. Rocher, A. Ougazzaden, A. Mircea, J. Appl. Phys. 75 (1994) 7881.
[18] R.D. Twesten, D.M. Follstaedt, S.R. Lee, E.D. Jones, J.L. Reno, J. Mirecki-Millunchick, S.P. Norman, A. Ahrenkiel, Phys. Rev., B 60 (1999) 13619.
[19] Z.F. Huang, R.C. Desai, Phys. Rev., B 65 (2002) 205419.
[20] J.D. Eshelby, Proc. R. Soc. London, Ser. A 241 (1957) 376.
[21] D.E. Jesson, S.J. Pennycook, J.M. Baribeau, D.C. Houghton, Phys. Rev. Lett. 71 (1993) 1744.
[22] A.A. Maradudin, R.F. Wallis, Surf. Sci. 91 (1980) 423.
[23] N. Sridhar, J.M. Rickman, D.J. Srolovitz, Acta Mater. 45 (1997) 2715.
[24] H.A. Macleod, Thin Film Optical Filters, 2nd edition, IOP Publishing, Bristal, Philadelphia, 2001, p. 179, Chap. 5.
[25] G. Binnig, C.E. Quate, Ch. Gerber, Phys. Rev. Lett. 56 (1986) 930.
[26] E. Meyer, H. Heinzelmann, P. Grütter, T. Jung, T. Weisskop, H. Hidber, R. Lapka, H. Rudin, J. Güntherodt, J. Microsc. 152 (1988) 269.

[27] H.P. Lang, M. Hegner, E. Meyer, Ch. Gerber, Nanotechnology 13 (2002) R29.
[28] E. Meyer, R. Lüthi, L. Howald, W. Gutmannsbauer, H. Haefke, H. Güntherodt, Nanotechnology 7 (1996) 340.
[29] U. Landman, W.D. Luedtke, N.A. Burnham, R.J. Colton, Science 248 (1990) 454.
[30] D. Ricci, M. Grattarola, J. Microsc. 176 (1994) 254.
[31] D. DeVecchio, B. Bhushan, Rev. Sci. Instrum. 68 (1997) 4498.
[32] D.H. Gracias, G.A. Somoraj, Macromolecules 31 (1998) 1269.
[33] P. Attard, J.L. Parker, Phys. Rev., A 46 (1992) 7959.
[34] J.A. Greenwood, Proc. R. Soc. Lond., A 453 (1997) 1277.
[35] J.P. Pethica, A.P. Sutton, J. Vac. Sci. Technol., A 6 (1988) 2400.
[36] U. Landman, W.D. Luedtke, N.A. Burnham, R.J. Colton, Science 248 (1990) 454.
[37] W. Chang, J. Hsu, T. Lai, J. Phys. D: Appl. Phys. 37 (2004) 1123.
[38] H. Hölscher, U.D. Schwarz, R. Wiesendanger, Appl. Surf. Sci. 140 (1999) 344.
[39] B.E. Shapiro, H. Qian, J. Therm. Biol. 194 (1998) 551.
[40] S.M. Foiles, M.I. Baskes, M.S. Daw, Phys. Rev., B 33 (1986) 7893.
[41] R.M. Lynden-Bell, Science 263 (1994) 1704.
[42] W.C. Herrmann, D.E. Morton, Appl. Opt. 32 (1993) 5673.
[43] S. Ogura, H.A. Macleod, Thin Solid Films 34 (1976) 371.
[44] C.J. Stolz, J.R. Taylor, W.K. Eickelberg, J.D. Lindh, Appl. Opt. 32 (1993) 5666.
[45] S. Yu, Terence K.S. Wong, K. Pita, X. Hu, V. Ligatchev, J. Appl. Phys. 92 (2002) 3338.
[46] A. van de Walle, M. Asta, P.W. Voorhees, Phys. Rev., B 67 (2003) 041308.
[47] N.K. Sahoo, S. Thakur, M. Senthilkumar, D. Bhattacharyya, N.C. Das, Thin Solid Films 440 (2003) 155.
[48] R.G. Munro, “Elastic moduli data for polycrystalline ceramics”, NISTIR 6853(2002) Gaithersburg, Maryland 20899.